Modelling and experimental verification of temperature effects on back electromotive force waveforms in a line start permanent magnet synchronous motor

Received 5 July 2021
Revised 26 November 2021
3 January 2022
Accepted 4 January 2022

Mariusz Baranski, Wojciech Szelag and Wieslaw Lyskawinski
Faculty of Control, Robotics and Electrical Engineering, Poznan University of Technology, Poznan, Poland

Abstract

Purpose – This paper aims to elaborate the method and algorithm for the analysis of the influence of temperature on back electromotive force (BEMF) waveforms in a line start permanent magnet synchronous motor (LSPMSM).

Design/methodology/approach – The paper presents a finite element analysis of temperature influence on BEMF and back electromotive coefficient in a LSPMSM. In this paper, a two-dimensional field model of coupled electromagnetic and thermal phenomena in the LSPMSM was presented. The influence of temperature on magnetic properties of the permanent magnets as well as on electric and thermal properties of the materials has been taken into account. Simulation results have been compared to measurements. The selected results have been presented and discussed.

Findings – The simulations results are compared with measurements to confirm the adequacy of this approach to the analysis of coupled electromagnetic-thermal problems.

Originality/value – The paper offers appropriate author's software for the transient and steady-state analysis of coupled electromagnetic and thermal problems in LSPMS motor.

Keywords Back electromotive force, Line start permanent magnet synchronous motor, FE methods, Coupled electromagnetic-thermal phenomena, Experimental verification, Electromagnetic fields, Permanent magnet machine, Thermal analysis, Numerical analysis

Paper type Research paper

1. Introduction

Line start permanent magnet synchronous motors (LSPMSMs) are characterized by a high value of power density, compact design as well as a high power factor and high efficiency. For this reason, they are commonly used in industrial applications replacing classic induction motors (Ganesan and Chokkalingam, 2019; Pałka *et al.*, 2019). When designing new LSPMSM constructions, sub-assemblies of classic induction motors are often used (Jedryczka *et al.*, 2014; Baranski *et al.*, 2017; Baranski *et al.*, 2020), and designing comes down

Funding: This research was funded by the Polish Government, grant number (0212/SBAD/0538).

COMPEL - The international journal for computation and mathematics in electrical and electronic engineering
Vol. 41 No. 5, 2022
pp. 1491-1504
Emerald Publishing Limited
0332-1649
DOI 10.1108/COMPEL-07-2021-0228

to developing a new structure of a rotor. When designing and optimizing a rotor with permanent magnets and a starting cage, it is important to choose the right shape and arrangement of magnets and cage winding bars (Yang *et al.*, 2008; Knypiński, 2017). The aim is to achieve the highest efficiency and power factor while ensuring requirements for starting parameters (Knypiński *et al.*, 2017). In addition, due to the minimization of electromagnetic torque ripples, the aim is to obtain the magnetic field distribution in the air gap and the $e(t)$ waveforms of back electromotive force (BEMF) with the lowest content of higher harmonics (Jedryczka *et al.*, 2014; Lin *et al.*, 2018).

Long-term operation of the motor at rated load conditions, its frequently repeated starting processes and direct reversing as well as its work at elevated ambient temperature can cause a large increase in the temperature of magnets and as a consequence, lead to:

- reduction of the voltage induced in the windings with increasing temperature, reduction of the electromagnetic torque; or
- a partial demagnetization of the magnets and permanent deterioration of the motor's functional parameters (McFarland and Jahns, 2012; Hamidizadeh *et al.*, 2016; Baranski *et al.*, 2017; Chen *et al.*, 2017).

A benchmark of the effect of temperature on the value of induced voltage can be the change of the k_E BEMF coefficient occurring with the change of temperature. This coefficient determines the value of the voltage induced in the winding per rotating of the rotor (Drury *et al.*, 2010; Ozturk *et al.*, 2010; Ma and Qi, 2018). The k_E coefficient is often applied in classical circuit models of permanent magnet machines. It is used, among other things, for the analysis and design of drive systems and the control or monitoring of their state (Ramakrishnan *et al.*, 2009; Ozturk *et al.*, 2010; Ma and Qi, 2018). For example, in permanent magnet synchronous motor drives, accurate knowledge of machine parameters like the k_E coefficient has the advantage of controlling and/or monitoring its condition. Disregarding the influence of temperature on the EMF value in these models and thus also on the k_E coefficient may lead to obtaining less reliable calculation results.

The decrease of the magnetic flux generated in the machine by the magnets that occurs with increasing temperature is due to the influence of temperature on the magnetic

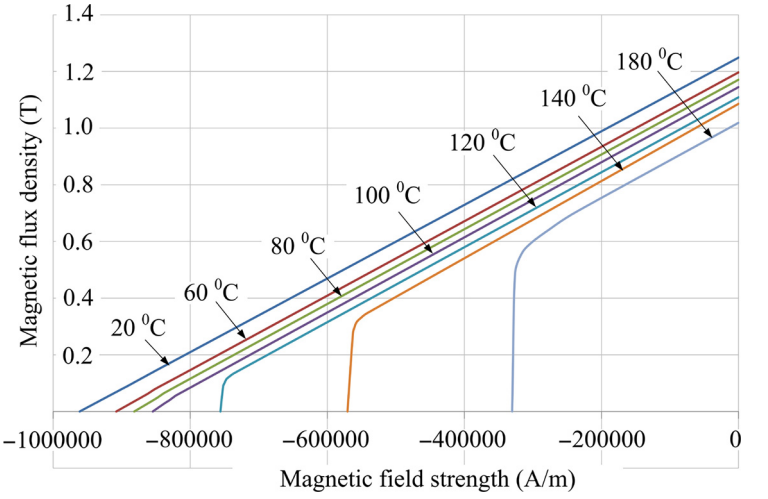

Figure 1.
Family of demagnetization characteristics $B(H, \tau_s)$ of magnetically hard N38SH material

properties of the magnetically hard material. The influence of temperature on magnetic properties of magnets is most often presented in catalogs of magnetically hard materials using a family of demagnetization characteristics. An example of a family of demagnetization characteristics is shown in Figure 1 (www.eclipsemagnetics.com).

The authors of the paper curried out simulation and experimental studies aimed at investigating the effect of temperature of the machine's components on the shape of the $e(t)$ waveform and on the value of the electromotive force in LSPMSMs. Moreover, the temperature dependence of the $k_E = E_{1max}/n$ coefficient, where E_{1max} is the amplitude of the fundamental harmonic of the voltage induced in the winding and n is the rotational rotor speed, was calculated. The calculations were carried out using the software developed by the authors for the field two-dimensional (2D) analysis of electromagnetic and thermal phenomena in the permanent magnet synchronous motor adopted to asynchronous starting (Baranski *et al.*, 2017, 2019, 2020). Experimental research was carried out on a specially constructed laboratory stand.

2. Mathematical model of electromagnetic and thermal phenomena of line start permanent magnet synchronous motors

The model developed by the authors, a 2D mathematical model of an LSPMSM has been presented in detail in Baranski *et al.* (2019, 2020). This model includes equations describing magnetic field distribution, thermal field distribution and mechanical equilibrium. It was assumed that the magnetic properties of the stator and rotor core, as well as permanent magnets, are due to equations $\boldsymbol{H} = \nu \boldsymbol{B}$ and respectively, $\boldsymbol{B} = \mu_0(\boldsymbol{H} + \boldsymbol{\theta}_m)$, where $\boldsymbol{B}$ is the vector of magnetic flux density, $\boldsymbol{H}$ is the magnetic field strength vector, $\boldsymbol{\theta}_m$ is the magnetization vector in the region with permanent magnets, ν is the magnetic reluctivity and μ_0 is the magnetic permeability of the vacuum. In the developed field model of thermal phenomena, the equation of the magnetic field is associated with the loop equations of the electrical circuits of the device and with the mechanical equilibrium equation of the drive system (Demenko, 1996; Driesen and Hameyer, 2002; Baranski *et al.*, 2019, 2020):

$$J_i \frac{\mathrm{d}^2 \gamma}{\mathrm{d}t^2} + T_L = T \tag{1}$$

where J_i is the moment of inertia of the movable elements of the system, γ is the angular position of the rotor, T_L is the load torque. The driving torque T is determined on the basis of the calculated magnetic field distribution (Demenko, 1996).

In the process of converting electrical energy into a mechanical one, power loss occurs, which is the source of heat in the machine. The temperature increase of the motor's components causes changes in the electrical, magnetic and thermal properties of materials (Baranski *et al.*, 2019, 2020). The temperature change significantly affects magnetic properties of permanent magnets (McFarland and Jahns, 2012; Baranski *et al.*, 2020). For this reason, the mathematical model of the motor has been fitted with an equation describing thermal phenomena (Baranski *et al.*, 2020):

$$\nabla Q + P_h = c_h \rho \frac{\mathrm{d}\tau}{\mathrm{d}t} \tag{2}$$

The heat capacity of the materials is established by the specific mass ρ and the specific heat capacity c_h. $Q = -k\nabla\tau$ is the conductive heat flux, where k is the thermal conductivity of the medium and τ is the temperature. P_h is the power-loss density. Convection heat transfer on the solid–fluid boundaries along the air gap is calculated considering the state of the airflow in the air gap (Baranski, 2019). The convection thermal coefficient in the outer surface of the frame was calibrated to match the temperatures measured at the motor frame (Baranski, 2019).

Numerical methods based on discretization of space and time are used to solve non-linear equations of the field model of coupled phenomena in an LSPMSM (Demenko, 1996). The FEM was used to determine magnetic field and temperature field distributions in the analyzed motor (Demenko, 1996; Driesen and Hameyer, 2002). For this purpose, the considered domain has been divided into triangular elements. After the discretization of time and using a backward differential scheme, a system of non-linear algebraic equations describing transient electromagnetic and thermal phenomena in the motor, taking into account the rotor's motion, was obtained:

$$\begin{bmatrix} \boldsymbol{G}(1-\boldsymbol{M})\Delta t^{-1} & 0 \\ -N^T & -\boldsymbol{L} \end{bmatrix} \begin{bmatrix} \varphi^{n-1} \\ i^{n-1} \end{bmatrix} + \begin{bmatrix} \boldsymbol{\theta}_m^n \\ -\Delta t U^n \end{bmatrix} = \\ = \begin{bmatrix} \boldsymbol{S}^n + G(1-\boldsymbol{M})\Delta t^{-1} & -N \\ -N^T & -(\boldsymbol{R}\Delta t + \boldsymbol{L}) \end{bmatrix} \begin{bmatrix} \varphi^n \\ \boldsymbol{i}^n \end{bmatrix} \tag{3}$$

$$\left(\boldsymbol{S}_\tau^n + \boldsymbol{K}_{\tau b}^n + \boldsymbol{M}_\tau^n \Delta t^{-1}\right) \boldsymbol{\tau}^n = \boldsymbol{P}^n + \boldsymbol{K}_{\tau o}^n + \boldsymbol{M}_\tau^n \Delta t^{-1} \boldsymbol{\tau}^{n-1} \tag{4}$$

$$J_i\left(\gamma^{n+1} - 2\gamma^n + \gamma^{n-1}\right)/(\Delta t)^2 = T^n - T_L^n \tag{5}$$

where $\boldsymbol{S}$ is the magnetic reluctance matrix, $\boldsymbol{\varphi}$ is the vector of potentials in nodes of the mesh, $\boldsymbol{i}$ is the vector of loop currents, $\boldsymbol{U}$ is the vector of supply voltages, $\boldsymbol{M}$ is the matrix of coefficients, $\boldsymbol{R}$ and $\boldsymbol{L}$ are the matrices of resistances and inductances of the windings and the supply system circuit, $\boldsymbol{N}$ is the matrix describing the number of turns assigned to the mesh nodes, $\boldsymbol{G}$ is the matrix of equivalent electrical conductances, $\boldsymbol{S}_\tau$ is the matrix of thermal conductances, $\boldsymbol{M}_\tau$ is the matrix of thermal capacitances, $\boldsymbol{\tau}$ is the vector of unknown temperatures, $\boldsymbol{P}$ is the vector of heat sources, $\boldsymbol{K}_{\tau b}$ and $\boldsymbol{K}_{\tau o}$ are the matrices of the coefficient describing heat transfer transport to the ambience of the motor. In the above relationships, $\Delta t = t_n - t_{n-1}$ is the length of a time-step, index n denotes the quantities of the actual time-step number $t = t_n$ and index $n-1$ denotes the previous time-step number $t = t_{n-1}$. For example: $\boldsymbol{S}^n = \boldsymbol{S}(t_n)$, $\boldsymbol{\varphi}^n = \boldsymbol{\varphi}(t_n)$.

In the developed model of electromagnetic-thermal phenomena, the distorted element method was used to map the rotor position change (Baranski *et al.*, 2017). The effect of temperature on elements of the vector $\boldsymbol{\theta}_m$ matrixes $\boldsymbol{R}$, $\boldsymbol{G}$ and $\boldsymbol{S}$ (Baranski *et al.*, 2019, 2020) was also taken into account.

The equations of the comprehensive discrete model, (3)–(5), are solved by using the Newton–Raphson procedure coupled with the block-over relaxation method (Baranski, 2019; Baranski *et al.*, 2020). Based on the presented algorithm, software for analyzing the effect of temperature on LSPMSM operations was developed. The software has been developed in the Borland–Delphi environment.

3. Tested motor and laboratory stand

Figure 2 shows the structure of the considered motor. The stator core shape of the mass-produced, general-purpose, 3-phase, 4 pole, 3 kW output power squirrel cage motor of Sg100L-4B type has been used.

There are 36 drop-shaped slots in the stator and 24 round slots in the rotor. NdFeB magnets of the N38SH type, *U*-shaped, are placed inside the rotor. The motor is supplied by a 3-phase balanced system of 400 V line to line voltage. The stator winding is made of winding wire with insulation class F and an allowable maximum temperature equal to 155°C. The motor rated parameters have been summarized in Table 1.

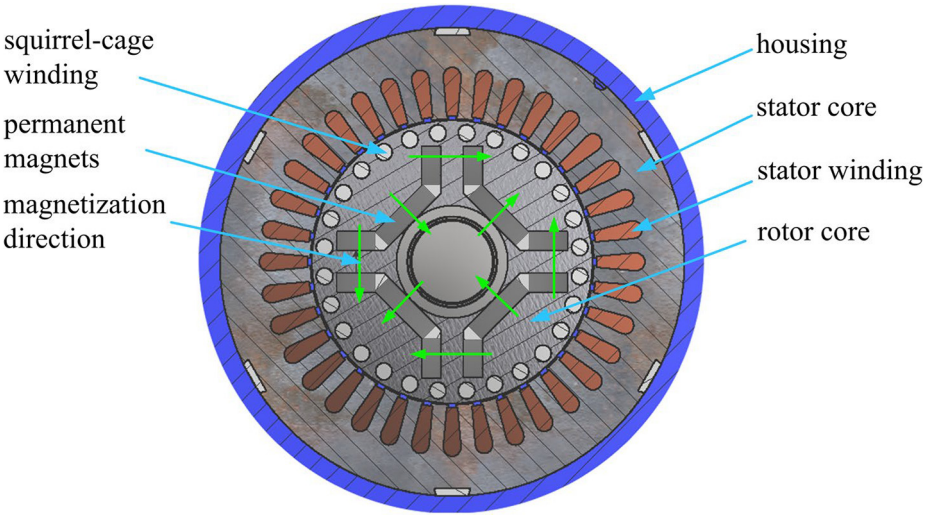

Figure 2.
Structure of the considered LSPMSM

P[kW]	U[V]	I[A]	f[Hz]
3.4	400	6.1	50

Table 1.
Data of LSPMSM

The developed test stand for determining the effect of temperature of magnets on voltage courses $e(t)$ induced in the stator winding is shown in Figure 3.

4. Results and discussions

The software developed by the authors was used to analyze the effect of temperature on the $e(t)$ waveform and BEMF value of the induced voltages in the stator windings. The

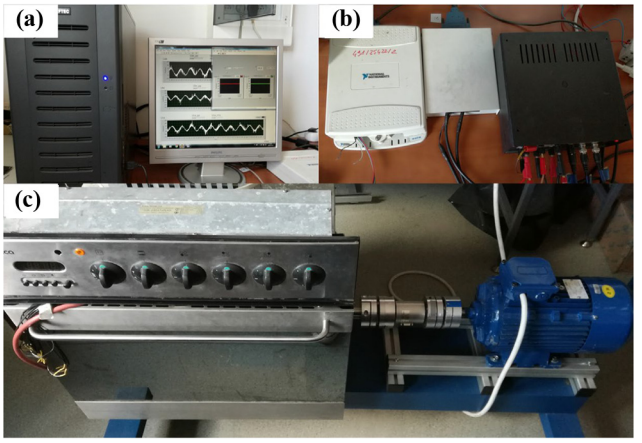

Notes: (a) Computer with PCI cards; (b) LEM transducer and NI analog/digital modules; (c) heating chamber

Figure 3.
Laboratory stand

calculations were carried out assuming that the rotor speed is equal to 1,500 rpm and no current flows in the stator winding. The obtained results of the simulation were compared to the results carried out under the same conditions of laboratory tests. Experimental studies were carried out on the computerized measuring stand developed and built by the authors – Figure 3. The tested LSPMS motor was placed in a heating chamber. The motor was driven by a squirrel-cage induction motor powered by a converter. The tests were carried out for several set temperatures of fixed components of the motor. These temperatures ranged from 26 to 140°C. The measurements were made after the temperature of the motor components was established. The waveforms were registered using measuring equipment of National Instruments Corporation. A detailed description of this apparatus is presented in Baranski (2019). It should be emphasized that the voltage tests were carried out on the motor after installing magnetized magnets in the rotor. Before the measurements of induced voltage, no motor starts were made and no current in the windings of the stator.

Figure 4 shows $e_{U\text{-}V}(t)$ waveforms of line-to-line voltages obtained on the basis of simulations (Figure 4a) and measurements (Figure 4b) for given values of the temperature τ_s. It was limited to showing only one of the three line-to-line voltages. The waveforms of the other line-to-line voltages have the same shape but are shifted in phase. The comparison of the motor $e_{U\text{-}V}(t)$ waveforms obtained on the basis of measurements and calculations is shown in Figure 5. The waveform of the induced voltage is affected by stator and rotor slots. The magnetic flux pulsations caused by the changing position of the stator slots relative to the rotor slots during the rotor's rotation, result in higher voltage harmonics. The results of the simulation and experimental studies confirm that as the temperature increases, both the magnetic flux generated by the magnets and the induced voltage decreases. It should also be noted that the temperature has little effect on the shape of the voltage waveform. Figure 6 presents higher harmonics for the selected temperatures τ_s included in the measured and calculated voltages. In addition to the basic harmonic, higher harmonics due to stator and rotor slots are visible. The differences between the amplitudes of individual voltage harmonics determined on the basis of measurements and simulation tests are caused, among others, by the use of a 2D model of phenomena, the assumed density of space and time discretization, as well as the imprecise mapping of real characteristics of soft and hard magnetic materials. The amplitudes of the harmonic $e_{U\text{-}V}(t)$ voltages obtained for given τ_s temperatures are shown in Figure 7. The calculated k_{E_C} and measured k_{E_M} coefficients obtained for given temperatures was summarized in Table 2. The results confirmed that the k_E coefficient decreases with the rise of temperature in stator winding.

To assess the discrepancy between the results of calculations and measurements (Figure 7), the factor $\chi_{E\%}$ was introduced, determining the relative difference between the harmonics' amplitudes of the measured and calculated voltages:

$$\chi_{E\%} = \frac{E_{1\max M} - E_{1\max C}}{E_{1\max M}} 100\% \tag{6}$$

where $E_{1\max M}$ and $E_{1\max C}$ are the amplitudes of the harmonic fundamental of the voltages $e(t)$ obtained from measurements and calculations, respectively. The calculated values of $\chi_{E\%}$ for the considered operation conditions have been summarized in Table 3. The table shows that the relative percentage difference between the results of the calculations and measurements does not exceed 3.80%.

To check whether high temperature permanently affected the voltage induced in the stator windings in the studied temperature range of magnets, the voltage waveforms were measured and compared:

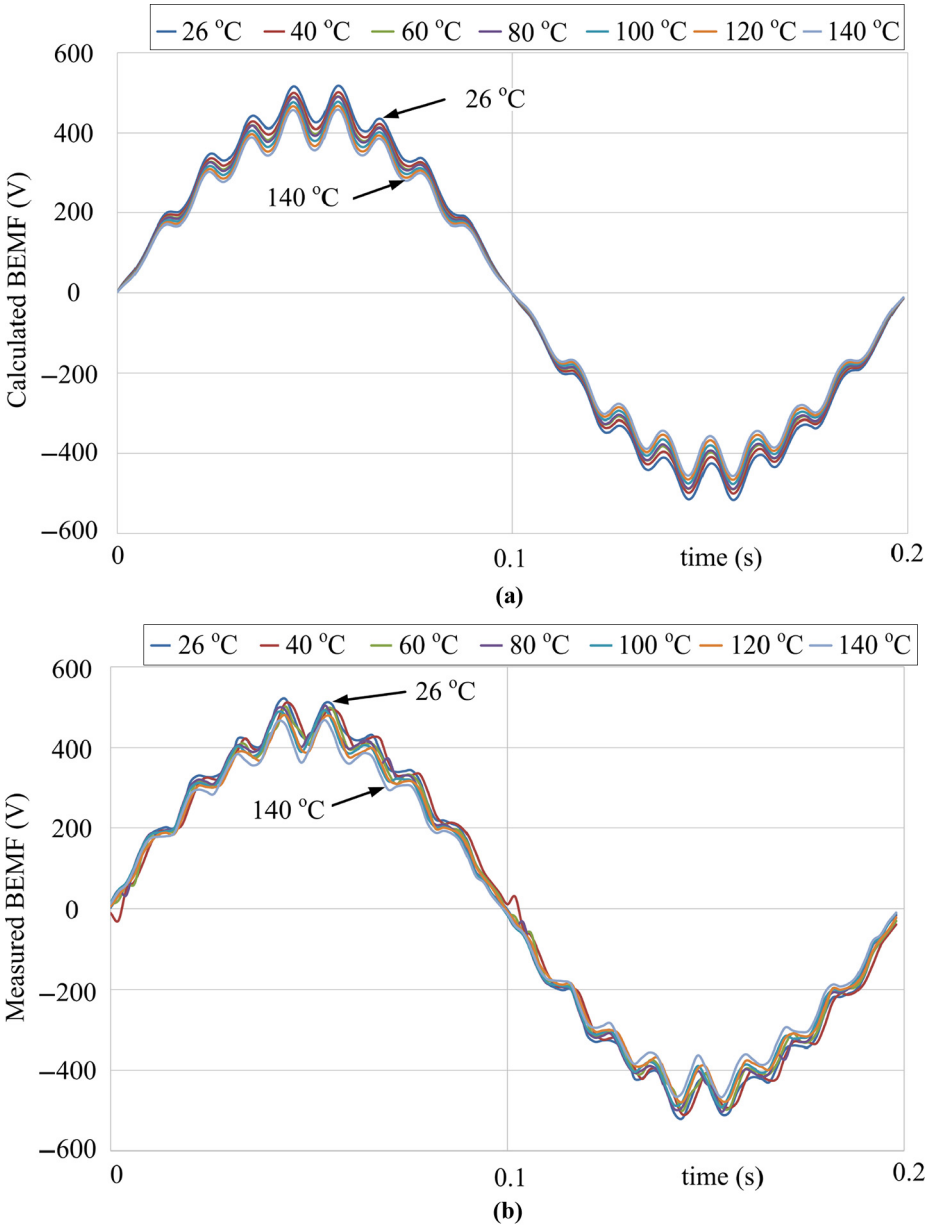

Notes: (a) Calculated and (b) measured for τ_s = 26ºC, τ_s = 40ºC, τ_s = 60ºC, τ_s = 80ºC, τ_s = 100ºC, τ_s = 120ºC and τ_s = 140ºC

Figure 4.
Back line-to-line electromotive forces $e_{U\text{-}V}(t)$ waveforms

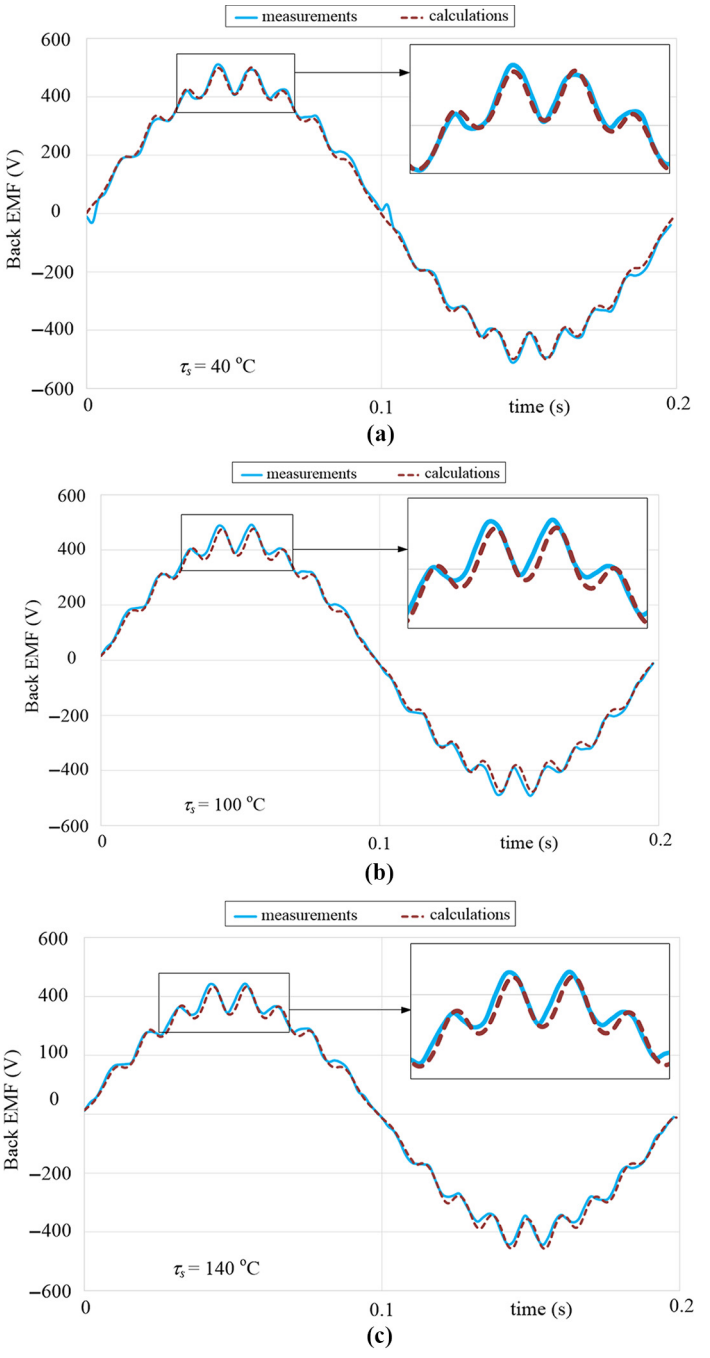

Figure 5.
Calculated and measured $e_{U\text{-}V}(t)$ waveforms for (a) τ_s = 40°C, (b) τ_s = 80°C and (c) τ_s = 140°C

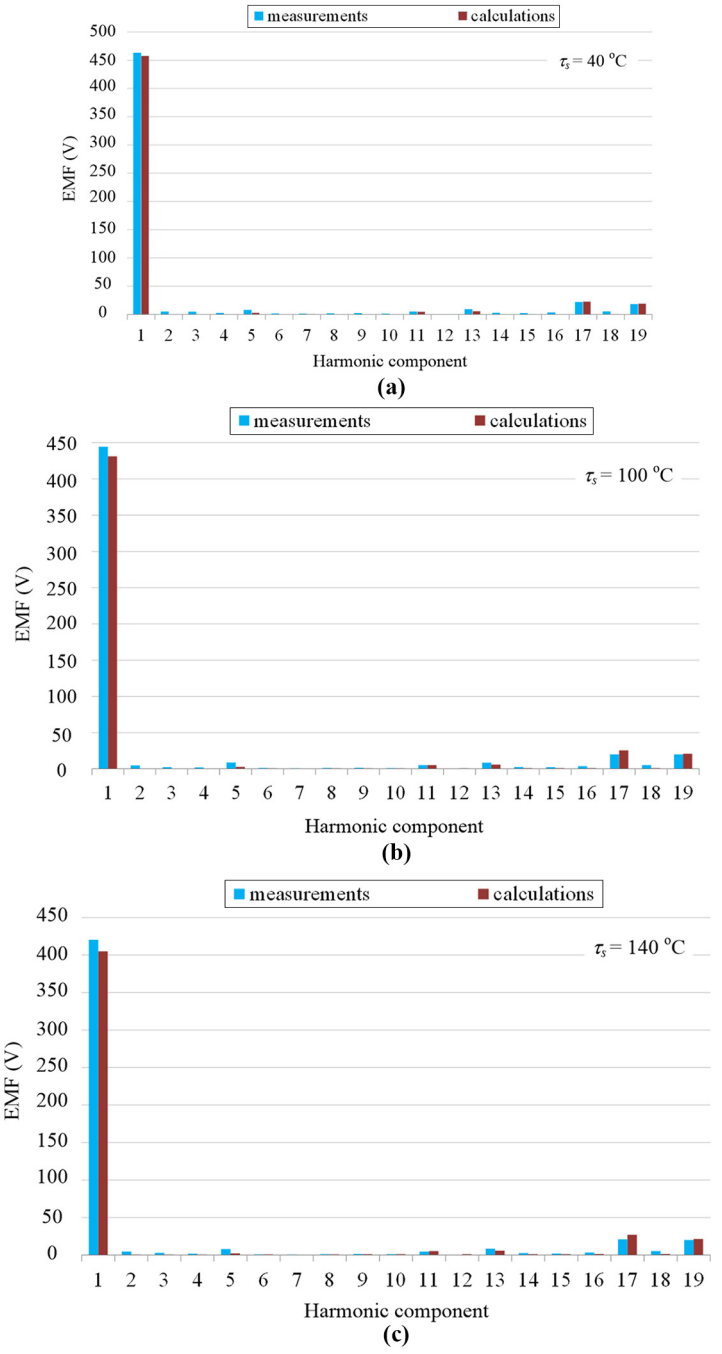

Figure 6.
Higher harmonics in calculated and measured $e_{U\text{-}V}(t)$ waveforms for (a) τ_s = 40°C, (b) τ_s = 80°C and (c) τ_s = 140°C

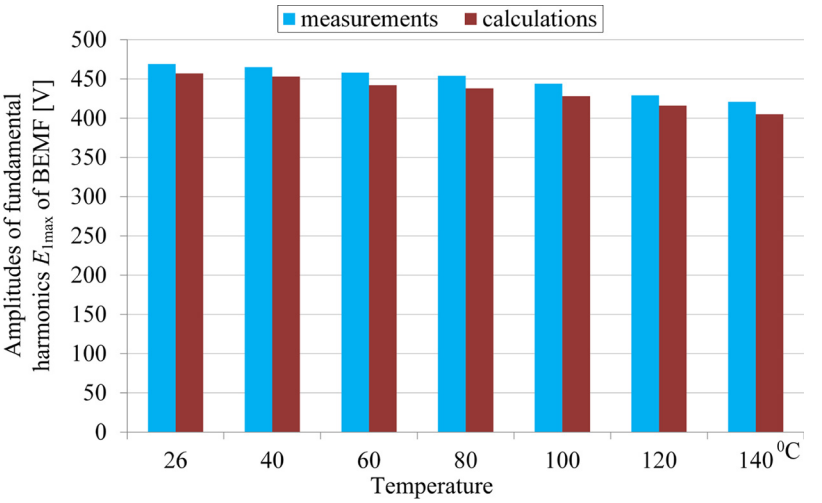

Figure 7.
Influence of temperature on amplitudes of fundamental harmonics of $e_{U\text{-}V}(t)$

Table 2.
The BEMF k_{E_M} and k_{E_C} coefficients depend on temperature

τ_s [°C]	26	40	60	80	100	120	140
k_{E_M} [V/rpm]	0.313	0.310	0.305	0.303	0.296	0.289	0.281
k_{E_C} [V/rpm]	0.305	0.302	0.295	0.292	0.285	0.277	0.275

Table 3.
Summary of the fundamental harmonic of the BEMF and BEMF coefficient $\chi_{E\%}$

τ_s [°C]	E_{1maxC} [V]	E_{1maxM} [V]	$\chi_{E\%}$ [%]
26	457	469	2.56
40	453	465	2.58
60	442	458	3.49
80	438	454	3.52
100	428	444	3.60
120	416	429	3.03
140	405	421	3.80

- after installing the magnets but before increasing the temperature of the machine; and
- during the course of the induced voltages after all tests related to heating the machine were performed.

The measurements of the voltage waveforms $e(t)$ before and after tests related to the heating of the machine were carried out at a temperature of $\tau_s = 26$°C. It should be emphasized that after mounting the magnets in the machine, only the temperature of the motor components was changed and the magnet flux was not stabilized by the inrush armature. The measurement results are presented in Figure 8.

The measured $e(t)$ waveforms show that the operation of magnets in the studied range of temperature changes from 26°C to 140°C and their repeated cooling to the ambient

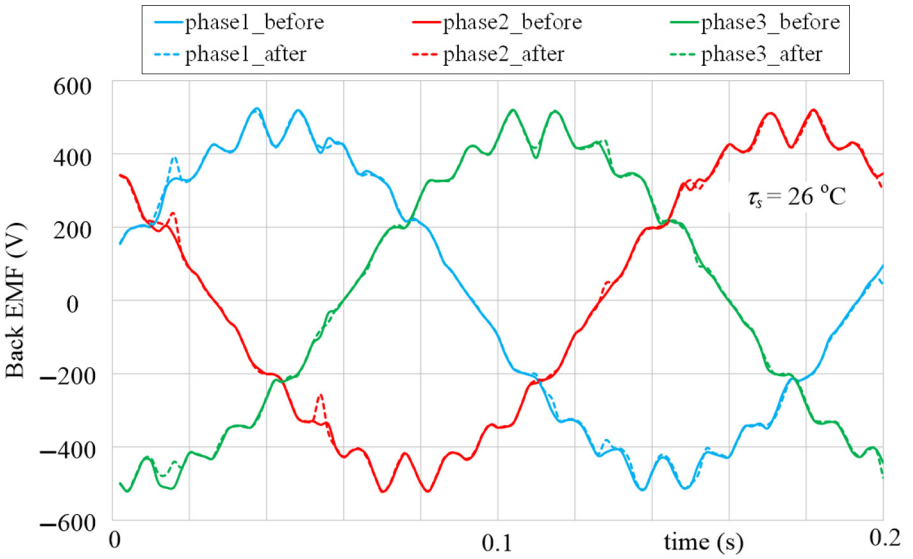

Figure 8.
Measured line-to-line *e(t)* waveforms for τ_s = 26°C before and after heating processes

temperature did little to affect the course and value of the induced voltages. It was found that after all the tests, the effective voltage value determined at 26°C decreased by approx. 0.4% in relation to the condition after the magnets were placed in the rotor.

Visible slight differences in the shape of the $e(t)$ waveforms induced before and after the tests at increased temperature are probably caused by the partial demagnetization of the magnet's sub-areas lying near the rotor bars (Baranski *et al.*, 2017). This phenomenon is associated with the pulsation of the magnet flux resulting from the grooving of the stator and rotor as well as with the currents induced in the rotor's rods by changes in this flux. As the temperature increases, the magnet resistance to demagnetization decreases, which adversely affects the process.

Due to the possibility of permanent and significant reduction of the magnet flux resulting in deterioration of the motor's functional parameters, experimental tests for $\tau_s > 140$°C were not carried out. The measurement was limited to simulation tests. The induced $e(t)$ waveforms in the LSPMSM with a magnet temperature of 180°C and 200°C, respectively, were analyzed. The induced line-to-line $e_{U\text{-}V}(t)$ waveforms were obtained and are presented in Figure 9. For comparison, the figure shows the $e_{U\text{-}V}(t)$ waveform obtained at a temperature of 140°C.

As expected, an additional temperature increase reduces the value of the fundamental amplitude of the harmonic of the electromotive force. The fundamental harmonic values obtained by the calculations are: $E_{1\max}(180°C) = 368$ V and $E_{1\max}(200°C) = 333$ V, respectively. As we can see, the magnetic properties of the permanent magnets have deteriorated significantly. This weakens the magnetic field generated by the magnets in an LSPMSM and reduces the value of both induced voltage and electromagnetic moment. A temperature of 150°C is the permissible operating temperature for N38SH magnets used in the motor.

To determine the relative percentage decrease in the value of the fundamental harmonic amplitude $E_{1\max}$, determined on the basis of calculations, the value of the coefficient $\Delta\alpha_{E\%}$, calculated on the basis of formula (7), is summarized in Table 4.

This factor determines the percentage change in $E_{1\max}$ that occurs with increasing temperature:

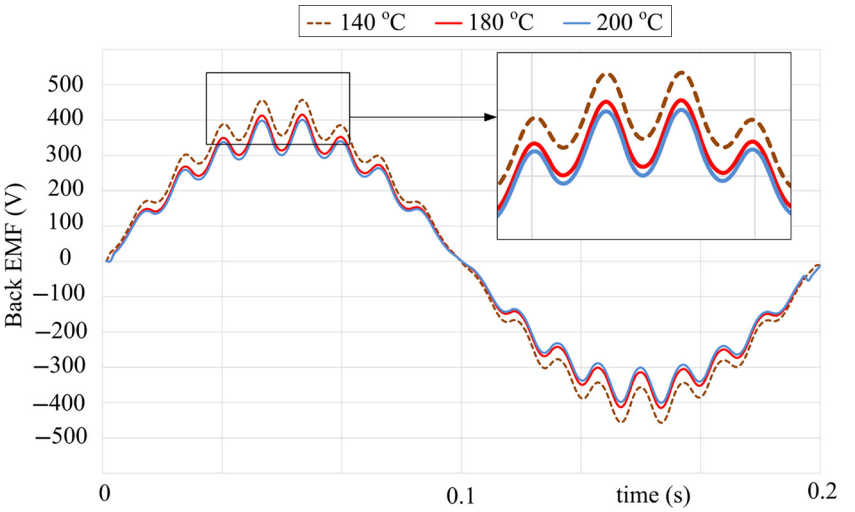

Figure 9.
Calculated $e_{U\text{-}V}(t)$ waveforms for $\tau_s = 140°C$, $\tau_s = 180°C$ and $\tau_s = 200°C$

τ_s [°C]	$\Delta\alpha_{E\%}$ [%]
40	0.88
60	3.28
80	4.16
100	6.56
120	9.19
140	11.30
180	19.47
200	27.13

Table 4.
Summary of the coefficient $\alpha_{E\%}$

$$\Delta\alpha_{E\%} = \frac{E_{1\max}(26°C) - E_{1\max}(\tau_s)}{E_{1\max}(26°C)} 100\% \quad (7)$$

where $E_{1\max}(26°C)$ is the value of the fundamental harmonic amplitude of the voltage $e_{U\text{-}V}(t)$ for the reference temperature of the motor components reaching 26°C, while $E_{1\max}(\tau_s)$ is the value of the fundamental harmonic amplitude of the voltage $e_{U\text{-}V}(t)$ for the set temperature τ_s.

For $\tau_s = 200$ °C, the relative decrease of $E_{1\max}$, with respect to the amplitude of the fundamental harmonic of the voltage induced in a temperature of 26°C, is approximately 27%.

5. Conclusions

The paper presents an analysis of the effect of temperature on the waveforms of the electromotive force induced in LSPMSM stator windings. The voltage induced in the machine during the generator's operation and the open circuit of the stator windings was investigated. The developed algorithm and program for analyzing the impact of temperature on the transient electromagnetic, thermal and mechanical phenomena in permanent magnet motors was used to conduct simulation tests. In an attempt to verify the results of the calculations for the induced voltage waveforms, a special laboratory stand has been constructed for this purpose. The tests were carried out for the given temperatures of the motor components. The survey showed good agreement between

the calculations and experimental tests. Thus, the reliability and usefulness of the developed software for analyzing the effect of temperature on the behavior of permanent magnet machines were confirmed. It should be emphasized that the obtained results could apply on the magnets type that are used in this research. Due to the different temperature dependence of the magnets, there is a probability that for other types of magnetic materials, the results can vary in magnitude of the measured and calculated electromotive force, but the main conclusions will be the same.

References

Baranski, M. (2019), "FE analysis of coupled electromagnetic-thermal phenomena in the squirrel cage motor working at high ambient temperature", *COMPEL – The International Journal for Computation and Mathematics in Electrical and Electronic Engineering*, Vol. 38 No. 4, pp. 1120-1132, doi: 10.1108/COMPEL-10-2018-0384.

Baranski, M., Szelag, W. and Jedryczka, C. (2017), "Influence of temperature on partial demagnetization of the permanent magnets during starting process of line start permanent magnet synchronous motor", *2017 International Symposium on Electrical Machines (SME). 2017 International Symposium on Electrical Machines (SME)*, pp. 1-6, doi: 10.1109/ISEM.2017.7993535.

Baranski, M., Szelag, W. and Lyskawinski, W. (2019), "An analysis of a start-up process in LSPMSMs with aluminum and copper rotor bars considering the coupling of electromagnetic and thermal phenomena", *Archives of Electrical Engineering*, Vol. 68 No. 4, pp. 933-946, doi: 10.24425/aee.2019.130693.

Baranski, M., Szelag, W. and Lyskawinski, W. (2020), "Analysis of the partial demagnetization process of magnets in a line start permanent magnet synchronous motor", *Energies*, Vol. 13 No. 21, p. 5562, doi: 10.3390/en13215562.

Chen, J., Wang, D., Cheng, S., Jiang, Y., Teng, X., Chen, Z., Shen, Y., Birnkammer, F. and Gerling, D. (2017), "A hysteresis model based on linear curves for NdFeB permanent magnet considering temperature effects", *IEEE Transactions on Magnetics*, Vol. 54 No. 3, pp. 1-5, doi: 10.1109/TMAG.2017.2763238.

Demenko, A. (1996), "Movement simulation in finite element analysis of electric machine dynamics", *IEEE Transactions on Magnetics*, Vol. 32 No. 3, pp. 1553-1556, doi: 10.1109/20.497547.

Driesen, J. and Hameyer, K. (2002), "Newton and quasi-Newton algorithms for non-linear electromagnetic–thermal coupled problems", *COMPEL – The International Journal for Computation and Mathematics in Electrical and Electronic Engineering*, Vol. 21 No. 1, pp. 116-125, doi: 10.1108/03321640210410788.

Drury, W.D., Holliday, D., Drury, D. and Mellor, P.H. (2010), "Adaptive sensorless position estimation of a field-weakened permanent magnet machine over an extended temperature range", pp. 223-223, doi: 10.1049/cp.2010.0110.

Ganesan, A.U. and Chokkalingam, L.N. (2019), "Review on the evolution of technology advancements and applications of line-start synchronous machines", *IET Electric Power Applications*, Vol. 13 No. 1, pp. 1-16, doi: 10.1049/iet-epa.2018.5283.

Hamidizadeh, S., Alatawneh, N., Chromik, R.R. and Lowther, D.A. (2016), "Comparison of different demagnetization models of permanent magnet in machines for electric vehicle application", *IEEE Transactions on Magnetics*, Vol. 52 No. 5, pp. 1-4, doi: 10.1109/TMAG.2015.2513067.

Jedryczka, C., Wojciechowski, R.M. and Demenko, A. (2014), "Finite element analysis of the asynchronous torque in LSPMSM with non-symmetrical squirrel cage winding", *International Journal of Applied Electromagnetics and Mechanics*, Vol. 46 No. 2, pp. 367-373, doi: 10.3233/JAE-141947.

Knypiński, Ł. (2017), "Optimal design of the rotor geometry of line-start permanent magnet synchronous motor using the bat algorithm", *Open Physics*, Vol. 15 No. 1, pp. 965-970, doi: 10.1515/phys-2017-0119.

Knypiński, Ł., Jedryczka, C. and Demenko, A. (2017), "Influence of the shape of squirrel-cage bars on the dimensions of permanent magnets in an optimized line-start permanent magnet synchronous

motor", *COMPEL – The International Journal for Computation and Mathematics in Electrical and Electronic Engineering*, Vol. 36 No. 1, pp. 298-308, doi: 10.1108/COMPEL-03-2016-0103.

Lin, M., Li, D., Zhao, Y., Ren, X. and Qu, R. (2018), "Comparison of different types of pole-changing line-start permanent magnet motors", *2018 XIII International Conference on Electrical Machines (ICEM)*, pp. 2051-2057, doi: 10.1109/ICELMACH.2018.8507188.

McFarland, J.D. and Jahns, T.M. (2012), "Investigation of the rotor demagnetization characteristics of interior PM synchronous machines during fault conditions", *2012 IEEE Energy Conversion Congress and Exposition (ECCE)*, pp. 4021-4028, doi: 10.1109/ECCE.2012.6342277.

Ma, Z. and Qi, X. (2018), "Permanent magnet motor temperature compensated constant torque control", *IFAC-PapersOnLine*, Vol. 51 No. 31, pp. 68-70, doi: 10.1016/j.ifacol.2018.10.013.

Ozturk, S.B., Alexander, W.C. and Toliyat, H.A. (2010), "Direct torque control of four-switch brushless DC motor with non-sinusoidal back EMF", *IEEE Transactions on Power Electronics*, Vol. 25 No. 2, pp. 263-271, doi: 10.1109/TPEL.2009.2028888.

Pałka, R., Woronowicz, K., Kotwas, J., Xing, W. and Chen, H. (2019), "Influence of different supply modes on the performance of linear induction motors", *Archives of Electrical Engineering*, Vol. 68, doi: 10.24425/aee.2019.129335.

Ramakrishnan, R., Islam, R., Islam, M. and Sebastian, T. (2009), "Real time estimation of parameters for controlling and monitoring permanent magnet synchronous motors", *2009 IEEE International Electric Machines and Drives Conference*, pp. 1194-1199, doi: 10.1109/IEMDC.2009.5075355.

Yang, G., Ma, J., Shen, J.-X. and Wang, Y. (2008), "Optimal design and experimental verification of a line-start permanent magnet synchronous motor", *2008 International Conference on Electrical Machines and Systems*, pp. 3232-3236.

About the authors

Mariusz Baranski received MS and PhD degrees in electrical engineering from Poznan University of Technology in 2002 and 2010. Currently, he is working for the Department of Mechatronics and Electrical Machines, Institute of Electrical Engineering and Electronics, Poznan University of Technology, Poznan, Poland. His areas of interest include finite-element simulation of static and dynamic electromagnetic and thermal phenomena in electric motors particular asynchronous and permanent magnet synchronous motors. Since 2010 he has been secretary of Editorial Board of Archives of Electrical Engineering. Mariusz Baranski is the corresponding author and can be contacted at: mariusz.baranski@put.poznan.pl

Wojciech Szelag received the MS, PhD and Doctor of Science degrees in Electrical Engineering from Poznan University of Technology in 1979, 1984 and 1998, respectively. Since 1982, he has been employed in research and education. He is currently a Professor of Electrical Engineering at Poznan University of Technology. He has published over 200 conference and journal papers on electrical machines, electromagnetics and electrodynamics. His research interests include electromagnetic field calculation, coupled electromagnetic-thermal and hydrodynamic phenomena analysis, design of electrical machines and actuators.

Wieslaw Lyskawinski received MS and PhD degrees in electrical engineering from Poznan University of Technology in 1990 and 1998. Currently, he is working for the Department of Mechatronics and Electrical Machines, Institute of Electrical Engineering and Electronics, Poznan University of Technology, Poznan, Poland. He deals with issues related to the analysis of operating states and the synthesis of pulse transformers and analysis of coupled electromagnetic, thermal and mechanical phenomena in electrical machines. His current research interests include design and analysis of permanent magnet motors and systems with magnetocaloric materials.